

# Influence of landslide geometry and kinematic deformation to describe the liquefaction of landslides: Some theoretical considerations

Th.W.J. van Asch\*, J.-P. Malet, L.P.H. van Beek

*Faculty of Geosciences, UCEL, P.O. Box 80.115, 3508 TC Utrecht, The Netherlands*

Received 14 June 2005; received in revised form 27 July 2006; accepted 18 August 2006  
Available online 27 September 2006

## Abstract

The generation of excess pore pressure and possible liquefaction can be explained by different mechanisms. In literature, less attention is given to the effects of landslide geometry and kinematic deformation on the generation of excess pore pressure and possible liquefaction of sliding blocks. The objective of this paper is to discuss these factors by proposing a simple analytical model of landslide liquefaction using classic soil mechanics theory. The model describes the initial state of failure and solves forces for each slice with the Bishop's limit equilibrium method. Immediately after failure the difference in movement for each slice is calculated assuming a viscous shear band and using the Coulomb-viscous model. The differential movements conduct to differential strains which are transferred to excess pore pressures. In slides characterized by curved slip surfaces, the lower parts showed compaction and increase in pore pressures during displacement, while the upper parts showed dilatation and a decrease in pore pressures. The potential liquefaction is then evaluated for each slice in relation to the displacement.

The model is applied to a slump-type failure that occurred on the Super-Sauze mudslide (Southeast France) in compact clay-rich material. It was observed that the slump completely liquefied into a flow. However, the model simulations were not able to completely liquefy all the slices of the slump in case a decrease in pore pressures through dilatation was assumed in the upper part of the slump. The decrease in pore pressures caused a rapid stabilisation of the remaining sliding body. In case a neutral pore pressure was assumed in the upper part with dilatation, movement and deformation of the remaining slices could continue leading to a nearly complete liquefaction of the slump.

Model simulations for many geometries of curved slip surfaces reveal that the liquefied volume increases with steeper slopes and more curved slip surfaces. It is discussed also how planar slides, which in theory show small differential movement of the individual slices and hence no large compaction, can completely liquefy through deformation at the toe.

© 2006 Elsevier B.V. All rights reserved.

*Keywords:* Fine-grained landslides; Kinematic deformation; Liquefaction; Stability analysis; Soil mechanics

## 1. Introduction

In order to explain and specify how slow-moving landslide transforms into debris flow, scientists and

engineers have elaborated comprehensive theories using well-established results from soil mechanics. In this view, the transformation from a landslide into a debris flow is depicted in three stages as underlined by [Ancy \(2001\)](#): (a) failure localized along a surface within a soil, generally described by the Mohr–Coulomb failure criterion, (b) partial or complete liquefaction of the material as a

\* Corresponding author.

E-mail address: [t.vanasch@geog.uu.nl](mailto:t.vanasch@geog.uu.nl) (Th.W.J. van Asch).

result of high pore-fluid pressure, (c) initiation and acceleration of the liquefied material. Although great effort has been devoted to the study of pore pressure generation and dissipation within a rigid landslide block, the understanding of fluidization of landslides due to differential movement and, hence, local compression in the moving body is as yet limited.

In this paper, liquefaction is defined as the process destroying the solid framework of a water-saturated sediment and creating a mixture with the behaviour of a liquid. From a mechanical view point, it represents the conditions where excess pore-fluid pressure in a soil mass is equal to the initial effective overburden.

There are several processes, which may generate liquefaction in coarse-grained or fine-grained sediments (Wang and Sassa, 2003). For coarse-grained, loosely packed low-density soils (typically sands or volcanic ashes), the most well known liquefaction mechanism is the collapse of the soil structure due to the rapid generation of large plastic strains by applying a given stress or load (Casagrande, 1971; Yoshimimi et al., 1989; Harp et al., 1990; Sasitharan et al., 1993; Anderson and Riemer, 1995). Several flume experiments have confirmed this mechanism of contraction of the soil structure for saturated materials in poorly drained conditions. For instance, the experiments of Iverson et al. (1997) in a 95-m-long channel, performed on coarse-grained loose soils consisting of poorly sorted sands and fine gravels, showed a dramatic increase in pore water pressure until liquefaction at all depths throughout the sliding block. Laboratory experiments carried out by Fuchu et al. (1999), Eckersley (1990) and Chu et al. (2003) on loose soils in essentially drained conditions showed the same mechanisms.

Mode of failure and initial bulk density seem to be first-order factors controlling liquefaction failure according to Wang and Sassa (2003). They carried out a number of laboratory flume tests on fine silica sand textures mixed with silts at different densities. The authors showed the influence of grain size on the optimal density for which there is contraction of the materials and a maximum pore-pressure build-up during and after failure. In addition, they clearly showed that pore pressures within saturated loose sandy textures increased with increasing velocities of the sliding block. Contracting behaviours related to changes in stresses have been observed also at the field scale for saturated materials (Olson et al., 2000). Contraction may also occur in case of unsaturated materials. Olivares et al. (2003) did several triaxial tests and laboratory flume experiments on loosely packed volcanic ashes, which failed by increase in saturation caused by rainfall infiltration and, consequently, reduction in suction strength. During wetting, the pyroclastic material

showed failure at rather low suction stresses but not complete saturation. However, drastic volume decrease occurs during failure, leading to saturation.

Apart from liquefaction induced by a contracting behaviour of the soil masses, the possibility of dilating behaviour prior to failure might also occur for dilative loose sands that lie below the critical-state line such as observed by Been et al. (1987), Fleming et al. (1989) and Harp et al. (1990).

Another mechanism causing liquefaction is related to the direction of the seepage forces of the groundwater flow. For instance, in infinite slope stability analyses, it is commonly assumed that the groundwater flow, and hence, the seepage force vector, is parallel to the topographical surface. Common theory in soil mechanics will show, however, that when the seepage force turns more and more in a direction opposite to gravity, effective stress progressively decreases, may become null and causes liquefaction of the sliding block (Nieuwenhuis, 1989; Iverson et al., 1997).

Another theory is related to the complex moving patterns of landslides. These landslides may have a net excess force down-slope generating acceleration of the moving block and, hence, an increase in translational kinetic energy. A part of this energy may be converted to kinetic vibration energy of agitated soil particles. According to Iverson et al. (1997), this energy can have a positive feedback on the liquefaction process in the landslide block. In flume experiments, it became clear that complete liquefaction occurred during runout of the material through agitation of the particles caused by the vibration energy and the development of intergranular pore pressures.

Finally, Sassa (1998) proposed another theory of landslide liquefaction. He hypothesized that shearing may break the soil particles near the slip surfaces causing a reduction of void ratio and possibly liquefaction.

Among these theories, less attention was given in the literature to the effects of landslide geometry and kinematic deformation in possible liquefaction of the sliding block. The hypothesis, on the basis of field evidence and literature review, is that excess pore pressures develop because compression zones and extension zones may arise in a moving body due to changes in slope gradient along the slip surface or by thrusts of newly failing slumping blocks in the upstream source area of the landslide. For instance, Okura et al. (2002) showed in a 9-m-long flume associating a steeper slope and a flatter slope, how the collapse of the soil on the steeper upslope part induced compression, liquefaction and a new slide in the lower less steep part. Savage and Smith (1986), Baum and Fleming (1991), Picarelli et al. (1995) and

Giusti et al. (1996) showed that internal deformation of slow-moving landslides results in positive or negative volumetric strain and hence the generation of negative or positive excess pore pressure under initially undrained conditions.

The objective of this paper is therefore to analyse the effect of geometry and kinematic deformation within a landslide body on the development of excess pore pressures and possible liquefaction. A simple analytical model of landslide liquefaction (2LM, Landslide Liquefaction Model) is proposed on the basis of classic soil mechanics theory. The model is applied to a slump-type failure that occurred on the Super-Sauze mudslide in Southeast France. Sensitivity of the model to changes in parameter values and landslide geometries are discussed.

## 2. The Landslide Liquefaction Model (2LM)

### 2.1. Model theory

The 2LM model is based on the theory of limiting equilibrium of soils and on constitutive laws. Fig. 1 depicts the forces on a typical slice, explains the scheme of the model and indicates the annotations used.

The stability of the rigid block is calculated with the method of slices, assuming a trial circular failure surface with the moving block divided into as many vertical slices so that the slip surface is approximately linear for each slice. The force balance is calculated with the Bishop's Simplified Method (Eq. (1)) which satisfies moment equilibrium and eliminates the effect of the inter-slice shear forces by assuming that the vertical component of the inter-slice forces is zero (Nash, 1987):

$$F = \frac{\sum_{i=1}^{i=n} [cl_i + (W_i - U_i) \tan \varphi]}{\sum W_i \sin \alpha_i} \frac{1}{m_{\alpha_i}} \quad (1)$$

$$m_{\alpha_i} = \cos \alpha_i \left( 1 + \tan \alpha_i \frac{\tan \varphi}{F} \right)$$

As the Bishop's equation is not explicit ( $F$  is on both sides of the equal sign), the equation is solved iteratively. The simulation starts by adjusting the pore-fluid pressure conditions in such a way that instability occurs in the rigid block at an overall safety factor chosen arbitrarily at a value lower than the unity. Pore-fluid pressure is introduced as a pore-pressure ratio value which is assumed to be equal for each slice in order to facilitate the adjustment to a certain safety factor value. The unstable conditions which are initially imposed create excess shear stresses that are then converted into displacements. During the movement, the driving force ( $D_i$ ), the pressure force ( $P_i$ )

and the resisting force ( $R_i$ ) are evaluated for each slice. It is assumed that the inertial term due to acceleration in the equation of motion can be neglected. Equilibrium between the remaining forces is reached in the following way (Fig. 1, Eq. (2)):

$$D_i + P_i - R_i = 0 \rightarrow R_i = D_i + P_i \quad (2)$$

The driving force  $D_i$  is defined by the parallel component of the weight for each slice (Eq. (3)):

$$D_i = W_i \sin \alpha_i \quad (3)$$

The pressure term  $P_i$  at the start of the movement is approximated by calculating the horizontal inter-slice net force  $\Delta E$  for each slice according to Bishop's Simplified Method. After failure, it is assumed that a thin viscous slip surface of thickness  $m$  and viscosity  $\mu$  develops. The velocity  $v_i$  of the sliding block (Eq. (4)) is then calculated from the resisting term  $R_i$  with the generalized Bingham (Coulomb viscous) model (Johnson, 1970) where  $R_i$  is defined by a yield strength dependent on the normal stress and on a viscous component:

$$R_i = S_i + \eta \frac{v_i}{m} l_i \rightarrow v_i = \frac{m}{\eta} \left( \frac{R_i - S_i}{l_i} \right) \quad (4)$$

$$S_i = cl_i + (W_i \cos \alpha_i - U_i) \tan \varphi$$

The displacement  $\Delta T_i$  during a time step  $\Delta t$  for a given slice is then given by Eq. (5):

$$\Delta T_i = v_i \Delta t \quad (5)$$

As we are not interested for our purpose in the absolute value of the velocity but only in the relative displacement  $\Delta T_i$  between the slices, it is assumed that the largest dominant strain component ( $\varepsilon_{xx}$ ) in the horizontal direction during the differential movement of the slices can be calculated by Eq. (6):

$$\varepsilon_{xx} = \frac{(\Delta T_{i+1} \cos \alpha_{i+1} - \Delta T \cos \alpha_i) + (\Delta T \cos \alpha_i - \Delta T_{i-1} \cos \alpha_{i-1})}{b_i} \quad (6)$$

Eq. (6) is in accordance with the definition that compressive strains are positive ( $\varepsilon_{xx} > 0$ ) and are related to positive compressive stresses, while dilative strains are negative ( $\varepsilon_{xx} < 0$ ) and are related to negative stresses. In a direction which makes an angle  $\theta$  with the axis of the largest principal strain, a relation can be found between the principal strains  $\varepsilon_x$ , the shear strain  $\varepsilon_{xy}$  and the normal strain  $\varepsilon_{xx}$  (Eq. (7)):

$$\varepsilon_x = \varepsilon_{xx} + \varepsilon_{xy} \frac{1 - \cos 2\theta}{\sin 2\theta} \quad (7)$$

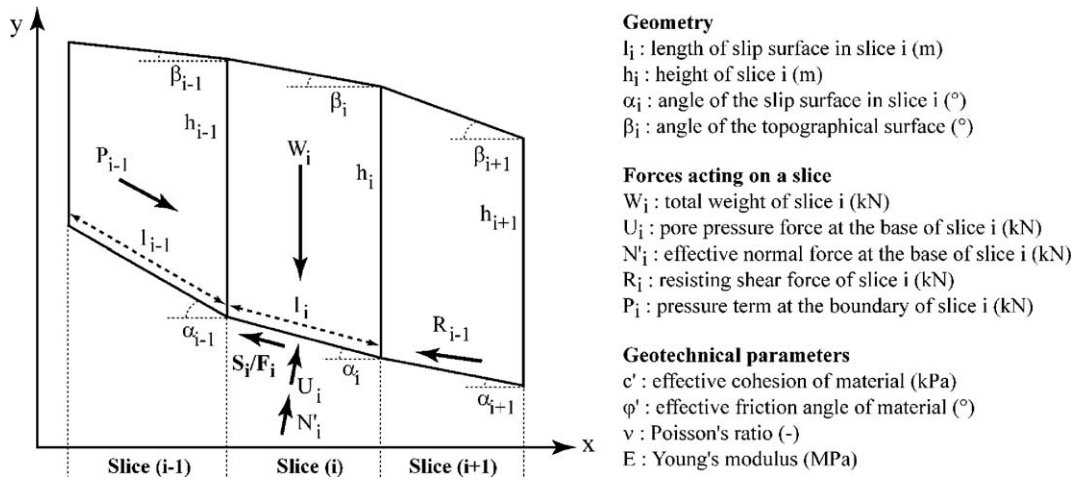


Fig. 1. Schematic force polygon for the Bishop's Simplified Method of limiting equilibrium and representation of the Landslide Liquefaction Model (2LM).

Since the amount of shear strain is ignored because it is difficult to separate it from rotation in slump failures ( $\epsilon_{xy}=0$  in Eq. (7)), hypothesis of equality between the principal strains and the normal strain is assumed (Eq. (8)):

$$\epsilon_x \approx \epsilon_{xx} \quad (8)$$

The changes in principal strain  $\epsilon_x$  are then translated to changes in principal total stress ( $\Delta\sigma_x$ ) with the same sign according to the following constitutive laws (Eqs. (9a) and (9b)):

$$\Delta\sigma_x = \frac{(\epsilon_x + \nu\epsilon_y)E}{(1-\nu^2)} \quad (9a)$$

$$\Delta\sigma_y = \frac{(\epsilon_y + \nu\epsilon_x)E}{(1-\nu^2)} = 0 \quad (9b)$$

where  $E$  is the Young's modulus (kPa) and  $\nu(-)$  is the Poisson's ratio. For nearly undrained conditions,  $\nu$  must be nearly 0.5. Totally undrained conditions cannot be assumed because in that case volumetric modulus of compressibility becomes infinite. In Eq. (9b), the changes in total stress in the  $y$ -direction ( $\Delta\sigma_y$ ) are ignored and the combination of Eqs. (9a) and (9b) delivers (Eq. (10)):

$$\Delta\sigma_x = \epsilon_x E \quad (10)$$

where  $E$  is the Young's modulus of a nearly undrained material. In case a saturated material, quasi-undrained loading conditions and no shear strain are assumed, the variation in pore-fluid pressure  $\Delta u$  can be described by Skempton's law (Smith and Smith, 1998) which in our case ( $\Delta\sigma_y=0$ ) reduces to (Eq. (11)):

$$\Delta u = (1+A)\Delta\sigma_x = (1+A)\epsilon_x E \quad (11)$$

where  $A$  is Skempton's pore-pressure coefficient. The pore pressure ratio  $r_u(-)$  for the slice  $i$  at time  $t$  is then given by Eq. (12):

$$r_{ui}^t = \frac{u_i^{t-1} + \Delta u_i^t}{h_i \gamma} \quad (12)$$

where  $\gamma$  is the bulk unit weight ( $\text{kN m}^{-3}$ ) of the saturated material. The variation in the value of the total lateral stress  $\Delta P_i$  during displacement is given by Eqs. (10) and (13):

$$\Delta P_i = \Delta\sigma_{xx} h_i \quad (13)$$

and is used to calculate  $P_i$  in the next time step. According to Hungr (1995), the pressure term  $P_i$  has ultimate values related respectively to the active and passive Rankine states. For a cohesive material with an inclined topographic surface, the Rankine states ( $p_p, p_a$ ) are estimated in terms of effective stress by Eq. (14) (Mazindrani and Ganjali, 1997):

$$p_p, p_a = \frac{\cos\beta}{\cos^2\phi} \{ [2\gamma z \cos^2\beta + 2c \cos\phi \sin\phi] \pm \sqrt{[4\cos^2\beta(\cos^2\beta - \cos^2\phi)\gamma^2 z^2 + 4c^2 \cos^2\phi + 8c\gamma z \cos^2\beta \sin\phi \cos\phi]} - \gamma z \cos\beta \} \quad (14)$$

The positive sign in Eq. (14) defines the passive Rankine state and the negative sign defines the active Rankine state. During motion, the active or passive Rankine states occur according to Eq. (15) (Hungr, 1995; Koch, 1998):

$$\text{active (+), passive (-) state} \begin{cases} \text{act if } \frac{\partial v}{\partial x} \geq 0 \\ \text{pass if } \frac{\partial v}{\partial x} < 0 \end{cases} \quad (15)$$

Eq. (15) indicates that if the velocities are increasing in a down-slope direction, dilatation occurs and the mass

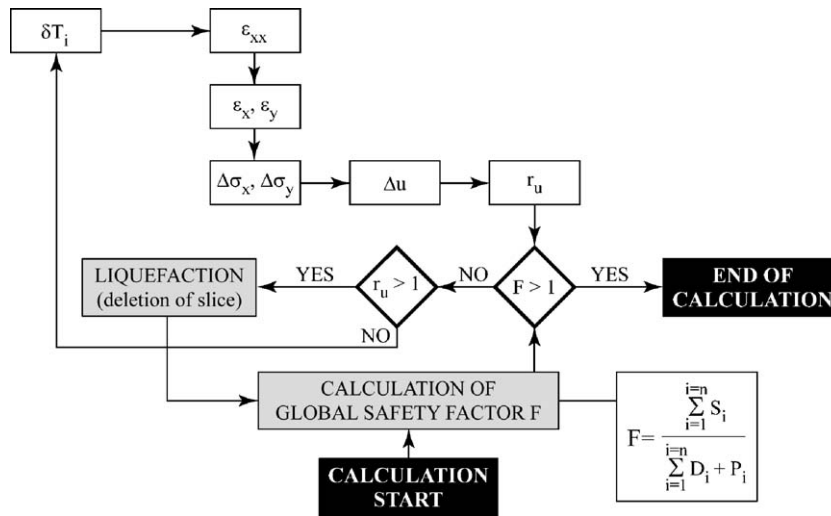


Fig. 2. Decision structure of the landslide liquefaction model 2LM.

transfers into an active Rankine state, while if velocities are decreasing in a down-slope direction, compaction occurs and the mass transfers into a passive Rankine state. The active and passive stresses of Eq. (14) can be integrated over depth according to Mazindrani and Ganjali (1997) which deliver the ultimate active and passive forces (Eq. (16)):

$$P_{i,+}^{ult} = \frac{1}{2} h_i p_{p,a} \quad (16)$$

### 2.2. Model decision structure

Fig. 2 gives an overview of the decision structure of the model. First, the initial global safety factor of the sliding block is calculated according to (Eq. (1)). In the model, the safety factor is manipulated by changing the

pore-fluid pressure conditions or the strength parameters to start the simulations with a safety factor arbitrarily set on a value of 0.98.

Then the displacements of the slices ( $\Delta T_i$ ) are calculated according to Eqs. (4) and (5). Due to the imposed differential displacements, the horizontal strains are calculated according to Eq. (6), to an updated value of the pore pressure ratio  $r_u$  (Eqs. (11) and (12)), to an updated value of the resisting force  $R_i$  (Eq. (4)) and to an updated value of the pressure term  $P_i$  (Eqs. (10) and (13)). A couple of decisions are taken at each step (Fig. 2) assuming that liquefaction of the slice occurs when the pore pressure ratio surpasses the value of 1:

- (1) In case both global safety factor and pore pressure ratio are below unity ( $F < 1, r_u < 1$ ), the displacement  $\Delta T_i$  is increased by a small increment of  $\Delta t$

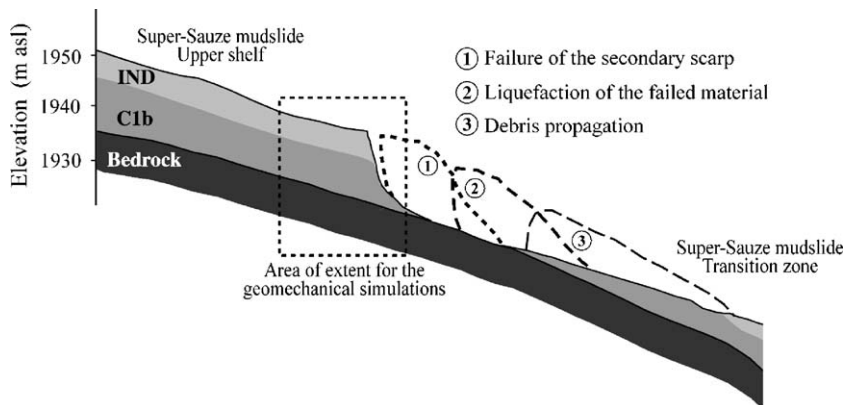


Fig. 3. Schematic sketch of a superficial slump-type failure observed on May 5, 1999 in the upper part of the Super-Sauze mudslide. The mudslide consists here of two materials :C1b is a silty-clay material and IND a silty-sand material.

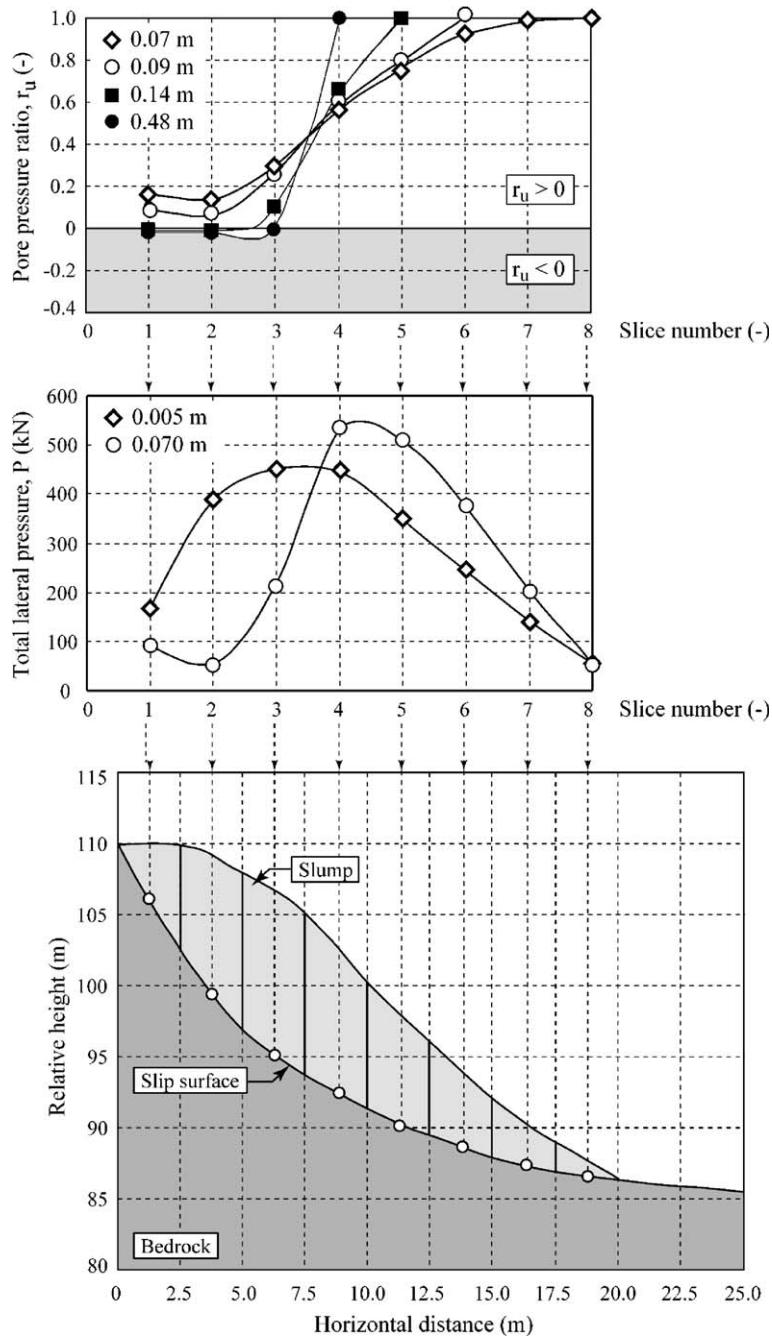


Fig. 4. Analysis of the Super-Sauze superficial slump with the 2LM model. (a) Development of pore-fluid pressure for the individual slices in relation to the mean displacement of the slump. A pore pressure ratio of  $r_u = 1$  indicates liquefaction of the slice. (b) Changes in total lateral stress of the slices during displacement. (c) Schematic geometry of the Super-Sauze slump used in the 2LM model.

according to Eq. (5) and the strain-stress field is re-calculated.

- (2) Due to the continuing incremental displacements, the global safety factor can surpass unity ( $F > 1$ ), and the moving block may become stable. In that

case, the simulations stop at an arbitrarily chosen safety factor of  $F = 1.1$ .

- (3) When the overall safety factor is below the unity ( $F < 1$ ), while in one slice the pore pressure ratio surpasses the unity ( $r_u > 1$ ), the liquefied slice is

Table 1

The Super-Sauze superficial slump: amount of displacement before stabilisation and corresponding amount of liquefaction for different values of  $C_s$  sand  $E$  with  $\nu=0.495$

$E$ (MPa)	$C_s$ (m <sup>2</sup> /kN)	Displacement (m)	Slice liquefied (number)	Percentage of total volume liquefied (%)
1.2	$3.3 \times 10^{-5}$ stiff clay	0.54	4–8	52.6
0.36	$0.5 \times 10^{-5}$ normal clay	1.60	4–8	52.6

deleted and a new global safety factor (without the liquefied slice) is calculated. If the updated overall safety factor remains below unity, the procedure is restarted by adding a new incremental displacement step  $\Delta T_i$ .

### 3. Field evaluation of 2LM: the case of the Super-Sauze mudslide

The Super-Sauze mudslide affects the north-facing slope of the Ubaye valley (Southeast French Alps), where the combination of steep slopes (up to 35°), down-slope stratigraphic dip of sensitive clay-shales (black marls) and the lack of vegetation make this basin one of the most landslide-, flow- and debris-flow-prone areas of Southeast France (Maquaire et al., 2003). The clay-rich Super-Sauze mudslide is characterized by a complex style of activity because of its capability to suddenly change behaviour. On the slow-moving mudslide (0.01–0.40 m day<sup>-1</sup>), superficial slumps can develop in secondary scarp, which may transform completely into muddy debris flows characterized by high velocities and runout distances. A dozen of events were observed in May 1999 on the site. Malet et al. (2003, 2005) have stressed that these muddy debris-flows, triggered in an impermeable stiff clay material, occur through a combination of heavy and sustained rainfalls, thawing soils and snowmelt.

The slump-type failure depicted in Fig. 3 completely liquefied into a muddy debris flow. A volume of material of 135 m<sup>3</sup> m<sup>-1</sup> (corresponding to a total volume of 2500 m<sup>3</sup>) failed suddenly from the secondary scarp of the mudslide and flowed rapidly on the hillslope. It is important to notice that in this period only small volume events were released (<5000 m<sup>3</sup>) from the large mudslide (750,000 m<sup>3</sup>). Nevertheless, morphological evidences and numerical simulations prove that the release of larger volumes is a realistic hazard scenario for specific climatic and hydro-geological conditions (Van Asch et al., 2004; Malet et al., 2005).

The Landslide Liquefaction Model (2LM) has been applied to analyse the liquefaction failure of the Super-Sauze superficial slump. Fig. 4a shows the development of pore-fluid pressure during movement assuming strength parameters of  $c=30$  kPa and  $\phi=32^\circ$ . Smith and Smith (1998) mentioned a compression coefficient for saturated stiff clays of  $3.3 \times 10^{-5}$  m<sup>2</sup> kN<sup>-1</sup>. These values were used to calculate the Young's modulus assuming a Poisson's ratio of 0.495 corresponding to a slightly compressive material. This delivers a Young's modulus value of  $E=1.2$  MPa, which lies in the range of normally consolidated clays. Fig. 4b indicates the successive liquefaction of the slices in the lower part of the moving block in relation to the mean displacement of the slices. Once a displacement of 0.07 m is reached, the two lowest slices (number 8 and 7) exhibit a pore-fluid pressure value of 1 and are liquefied. The slices numbers 6, 5 and 4 liquefied after a displacement of, respectively, 0.09 m, 0.14 m and 0.48 m. After a further displacement, the global safety factor reached a value of 1.1 and the simulation is stopped. The upslope slices exhibit a decrease in pore-fluid pressure due to dilation. The minimum pore-fluid pressure is arbitrarily set at zero. It is doubtful that very negative suction may be generated due to the development of fissures in this dilative section, and a temporary increase in stability in the upper part of the slope is expected due to this decrease in pore-fluid pressure. Fig. 4b indicates the changes in total lateral stress due to the differential displacement of the individual slices with an increase in the lower part and a decrease in the upper part.

The results are also summarised in Table 1 showing that about 50% of the material will liquefy after a displacement of 0.54 m. Table 1 also indicates that for a normal clay with a lower compression coefficient  $C_s$  (Smith and Smith, 1998) and a lower Young's modulus ( $E=0.36$  MPa) a larger displacement of 1.6 m is necessary to arrive at the same volume of liquefied material before stabilisation.

The 2LM simulations indicated, therefore, that about half of the Super-Sauze superficial slump may liquefy,

Table 2

Amount of displacement and liquefaction before stabilization for landslide with different slip surface curvatures and slope angles

Slope gradient (°)	Radius of slip circle (m)	Displacement before stopping (m)	Slice liquefied (number)	Percentage of total volume liquefied (%)	$c'$ (kPa)	$\phi'$ (°)
16	97.5	3.5	6–12	62.2	4.6	20
12	97.5	2.1	7–12	55.2	2.5	20
16	160	1.7	7–12	56.8	3.5	20
12	160	2.4	8–12	46.2	2.3	20

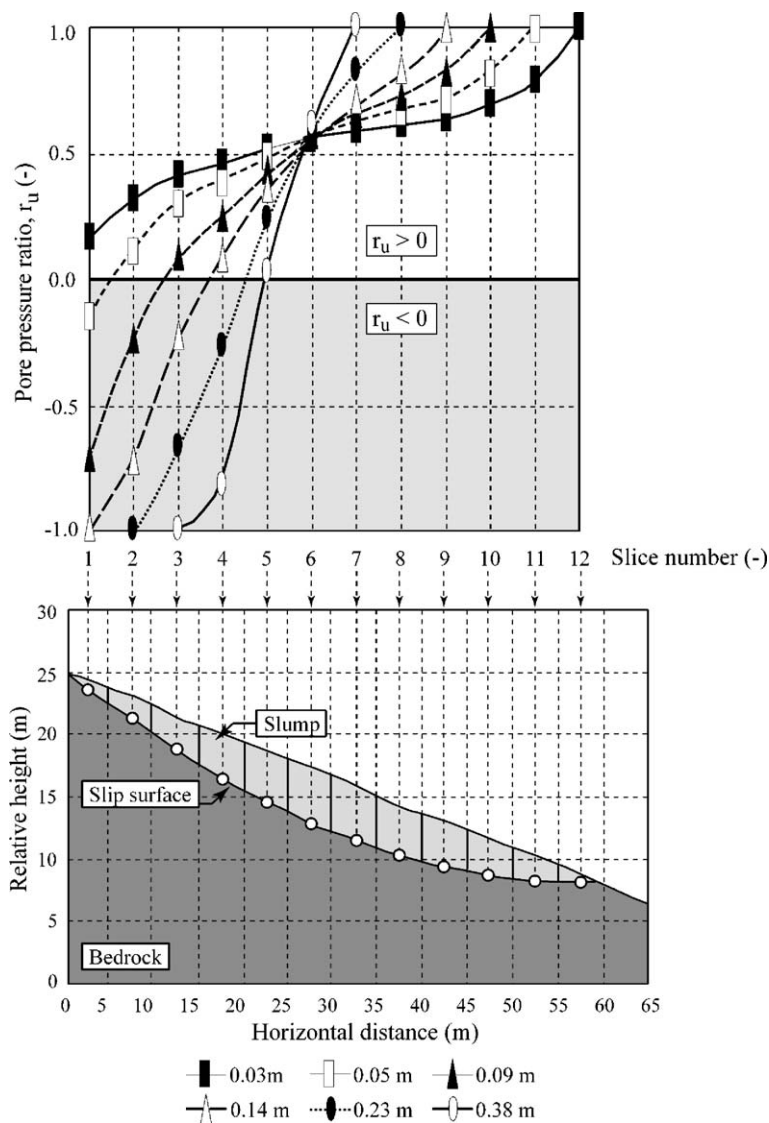


Fig. 5. Development of pore-fluid pressure for the individual slices in relation to the mean displacement of a landslide with a steep slope ( $16^\circ$ ) and a curved slip surface (radius of slip surface 97.5 m (see also Table 2).

while observations showed a nearly 100% of liquefaction (Malet et al., 2005). It is hypothesized that the stabilisation of the remaining part of the slump is probably not correctly simulated. This may be caused by the calculated decrease in pore pressure towards zero in the upper part of the dilating slump which adds too much strength and, hence, too much stability. Decrease in pore pressure may rapidly vanish or may not be generated in the dilatation zone due to the formation of fissures. That means that the upper part under more neutral pore-fluid pressure conditions still could move further downwards, deform and partly liquefy. A simulation was carried out for the Super-Sauze superficial slump (Fig. 4c) in which it was assumed neutral

pore-fluid pressures in the dilating zone. In that case, the upper part remains unstable and could move downwards leading to the liquefaction of slice number 3 (after a displacement of 2.82 m) and of slice number 2 (after a displacement of 5.18 m) (Fig. 4b,c). With this assumption, nearly 93% of the superficial slump has liquefied.

#### 4. The role of landslide geometry on landslide liquefaction

Since this paper discusses the role of landslide geometry in the development of excess pore-fluid pressure, four hypothetical landslide geometries were analysed.

Two geometries consisted of a slump-type landslide on a 16°-slope with two circular slip surfaces with a radius of, respectively, 97.5 m and 160 m. Two geometries were designed for a landslide on a 12° slope with two slip circles, which have the same radius as on the 16° slope (Table 2). The landslide materials are assumed to be fully saturated; the friction angle  $\phi$ -value is set at 20° while the cohesion  $c$  was adapted in such a way that the global safety factor at the start of movement was 0.98 (Table 2). Simulations were carried out for  $E=1.2$  MPa and  $\nu=0.495$ . The movement stops at a safety factor of 1.1.

Fig. 5 shows the development of pore-fluid pressure in relation to movement for the steeper slope (16°) with the more curved slip circle (radius 97.5 m). As shown already in Fig. 4, 2LM indicates that a landslide along a curved slip surface creates dilatation (negative strain) and hence lowering of the pore-fluid pressures from the initial neutral pressure ( $r_u=0.56$ ) in the upper part; in the lower part, displacements lead to compression and to an increase in pore-fluid pressures until liquefaction. In that case, the negative suction is given a minimum ( $r_u=-1$ ) because it is assumed that there is a limitation on the generation of suction due to the development of fissures in the dilatation zone. Fig. 5 indicates that slice numbers 6–12 are liquefied before the landslide stops at the arbitrarily overall safety factor of 1.1.

Table 2 suggests that with the same topographical slope angle, more curved slip surfaces generate more liquefaction. The same holds for a constant curvature but steeper topographical slopes. As a consequence, one can state that strongly curved slip surfaces on steeper slopes generate increasing liquefied volumes. One can expect from the above simulations on curved slip sur-

Table 3

Liquefaction of slices in relation to the displacements for a shallow translational slump with a bending slip surface at the toe

Displacement before liquefying (m)	Slice liquefied (number)
0.08	11–12
1.65	9–10
3.04	8

faces that shallow landslides, which have straight slip surfaces more or less parallel to the topographical surfaces, will show limited compression or dilatation and, therefore, will exhibit no liquefaction. However, there are many examples where these superficial shallow landslides transform into flows. One of the reasons might be that deformation occurs at the toe of the landslide where the slip surfaces show a curve towards the topographical surfaces.

Therefore, a straight slope with a straight slip surface characterized by a curvature at the toe and, thus, flattening of the slip surface angle (Fig. 6) was analyzed. The slope was divided into 12 slices, labelled from the top downwards. Both slip surface and topographical surface have an angle of 18.4°. At slice number 8, the slip surface angle starts to flatten until an angle 10.2° at the ultimate toe. The landslide material is saturated; strength parameters of  $c=5.5$  kPa and  $\phi=20^\circ$  allow the slope to be unstable. Table 3 indicates that the slices numbers 8–12 located at the bending slip surface will liquefy after a displacement of 3.04 m. The slope remains unstable and the slices located upslope are also able to liquefy when they arrive at the bending part and have the possibility to move further. For example, slice no. 8 has to travel 2.58 m to arrive at the bending part of the slip surface and to be compressed.

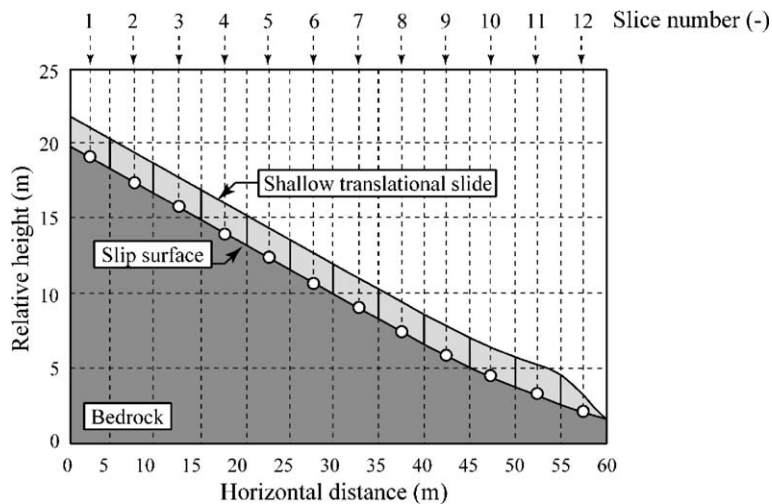


Fig. 6. Profile of a straight slip surface with a bending part at the toe.

## 5. Discussion and conclusions

Landslide liquefaction is not only generated by the volumetric collapse of loosely packed, coarse-grained material. Liquefaction may also occur as well in dense fine-grained material as, for example, the remoulded material of the clay–shale outcrops of Southeast France, through deformation and compression of the moving block.

According to the theoretical concept described in this paper, differences in displacements result in negative strains (dilation) in the upper parts of the landslides, while in the lower parts, positive strains are generated and, hence, compression which under undrained conditions may result into liquefaction. According to this concept, only a part of the moving block is able to liquefy.

The amount of liquefaction on a curved slip surface depends on the position of the point along the slope where downslope slices exhibit smaller displacements than upslope slices, creating compression. This amount of compression depends also on the curvature of the slip surface creating large differences in displacements between the slices. The 2LM simulations suggest that liquefaction increases with steeper slopes and more curved slip surfaces.

The 2LM model also shows possibilities for liquefaction of shallow planar soil slumps. Liquefaction of these landslides starts at the toe where the overall straight slip surface, due to kinematic constraints, has to show some bending in order to jump out of the more stable regolith or soil mantle downslope. Liquefaction at the toe increases the instability of the upper part of the landslide with the straight slip surface. This upper part further slides down and become compressed at the toe zone with the flattening (curved) slip surface resulting in further liquefaction.

The 2LM simulations indicate that about half of the Super-Sauze superficial slump liquefied, while observation showed a nearly 100% liquefaction. Nearly total liquefaction could be simulated by assuming that a decrease in pore-fluid pressure in the dilatative zone does not occur due to the formation of tension cracks. However, in the case of Super-Sauze, possible infill of melt water in tensile fissures in the dilatation zone in the upper part of the slump may have caused the total mobilization and liquefaction of the sliding material.

The 2LM model is very conservative in the way that no dissipation is allowed during deformation and failure. At this stage of development, dissipation is not considered in the model because one has to know the time period of movement and deformation to analyse the effect of pore-fluid dissipation. Besides the process of dissipation, pore-fluid pressure may be maintained or

even increased during movement due to vibration energy of the grains. The model describes, however, the relative role of landslide geometry and kinematic deformation on the generation of excess pore pressure. It explains why fine-grained rotational and translational slides may show more or less flow-like features at the toe through complete or partial liquefaction. Laboratory flume tests in progress should allow verifying the here-explained theory.

## References

- Ancey, C., 2001. Debris flows and related phenomena. In: Balmforth, N.J., Provenzale, A. (Eds.), *Geomorphological Fluid Mechanics*. Springer-Verlag, Heidelberg, pp. 528–547.
- Anderson, S.A., Riemer, M.F., 1995. Collapse of saturated soil due to reduction in confinement. *Journal of Geotechnical Engineering, American Society of Civil Engineers* 121 (2), 216–220.
- Baum, R., Fleming, R.W., 1991. Use of longitudinal strain in identifying driving and resisting elements in landslides. *Geological Society of America Bulletin* 103, 1121–1131.
- Been, K., Conlin, B.H., Crooks, J.H.A., Fitzpatrick, S.W., Jefferies, M.G., Rogers, B.T., Shinde, S., 1987. Back analysis of the Nerlerk berm liquefaction slides: discussion. *Canadian Geotechnical Journal* 24, 170–179.
- Casagrande, A., 1971. On liquefaction phenomena, Report of Lecture to British Geotechnical Society. *Geotechnique* 21 (3), 197–202.
- Chu, J., Leroueil, S., Leong, W.K., 2003. Unstable behaviour of sand and its implication for slope stability. *Canadian Geotechnical Journal* 40, 873–885.
- Eckersley, J.D., 1990. Instrumented laboratory flowslides. *Geotechnique* 40, 489–502.
- Fleming, R.W., Ellen, S.D., Albus, M.A., 1989. Transformation of dilatative and contractive landslide debris into debris flows: an example from Marin County, California. *Engineering Geology* 27, 201–223.
- Fuchu, D., Lee, C.F., Sijing, W., Yuong, F., 1999. Stress–strain behaviour of loosely compacted volcanic-derived soil and its significance to rainfall-induced fill slope failures. *Engineering Geology* 53 (3–4), 359–370.
- Giusti, G., Iacarino, G., Pellegrino, A., Russo, C., Urcioli, G., Picarelli, L., 1996. Kinematic features of earthflows in Southern Apennines, Italy. *Proceedings of the 7th International Symposium on Landslides, Trondheim, Balkema*, vol. 1, pp. 457–462.
- Harp, E.W., Weels, W.G., Sarmiento, J.G., 1990. Pore pressure response during failure in soils. *Geological Society of America Bulletin* 102 (4), 428–438.
- Hungry, O., 1995. A model for the runout analysis of rapid flow slides, debris flows and avalanches. *Canadian Geotechnical Journal* 32, 610–623.
- Iverson, M., Reid, M.E., LaHusen, R.G., 1997. Debris flow mobilization from landslides. *Annual Review of Earth and Planetary Sciences* 25, 85–138.
- Johnson, A.M., 1970. *Physical Processes in Geology*. Freeman, New York. 577 pp.
- Koch, T., 1998. Testing various constitutive equations for debris flow modelling. *IAHS Publication* 248, 249–257.
- Malet, J.-P., Remaitre, A., Maquaire, O., Ancey, C., Locat, J., 2003. Flow susceptibility of heterogeneous marly formations. Implications for torrent hazard control in the Barcelonnette basin (Alpes-

- de-Haute-Provence, France). Proceedings of the 3rd International Conference on Debris-Flow Hazard Mitigation, Mechanics, Prediction and Assessment, Davos, Millpress, vol. 1, pp. 351–362.
- Malet, J.-P., Laigle, D., Remaître, A., Maquaire, O., 2005. Triggering conditions of debris-flows associated to complex earthflows. The case of the Super-Sauze earthflow (South Alps, France). *Geomorphology* 66 (1–4), 215–235.
- Maquaire, O., Malet, J.-P., Remaître, A., Locat, J., Klotz, S., Guillon, J., 2003. Instability conditions of marly hillslopes: towards landsliding or gullying? The case of the Barcelonnette Basin, South East France. *Engineering Geology* 70 (1–2), 109–130.
- Mazindrani, Z.H., Ganjali, M.H., 1997. Lateral earth pressure problem of cohesive backfill with inclined surface. *Journal of Geotechnical and Geoenvironmental Engineering, American Society of Civil Engineers* 123 (2), 110–112.
- Nash, D.F.T., 1987. A comparative review of limit equilibrium methods of stability analysis. In: Anderson, M.G., Richards, K.S. (Eds.), *Slope Stability, Geotechnical Engineering and Geomorphology*. Wiley, pp. 11–77.
- Nieuwenhuis, J.D., 1989. *Inleiding Grondmechanica*. Faculty of Geosciences, Utrecht University. 54 pp.
- Okura, Y., Kithahara, H., Ochiai, H., Sammori, T., Kawanami, A., 2002. Landslide fluidisation process by flume experiments. *Engineering Geology* 66, 65–78.
- Olivares, L., Damiano, E., Picarelli, L., 2003. Wetting and flume tests on volcanic ash. Proceedings of the International Conference on Fast Slope Movements, Prediction and Prevention for Risk Mitigation, Naples, Pàtron Editore, pp. 399–404.
- Olson, S.M., Starck, T.D., Walton, W.H., Castro, G., 2000. 1907 static liquefaction flow failure of the north dike of Wachusett dam. *Journal of Geotechnical and Geoenvironmental Engineering, American Society of Civil Engineers* 126 (12), 1184–1193.
- Picarelli, L., Russo, C., Urcioli, G., 1995. Modelling earthflow movement based on experiences. Proceedings of the 11th European Conference on Soil Mechanics and Foundation Engineering, Copenhagen, Balkema, vol. 6, pp. 157–162.
- Sasitharan, S., Robertson, P.K., Sege, D.C., Morgenstern, N.R., 1993. Collapse behaviour of sand. *Canadian Geotechnical Journal* 30, 569–577.
- Sassa, K., 1998. Mechanisms of landslide triggered debris flow. In: Sassa, K. (Ed.), *Environmental Forest Science*. Kluwer, Dordrecht, pp. 471–490.
- Savage, W.Z., Smith, W.K., 1986. A model for the plastic flow of landslides. US Geological Survey Professional Paper 1385 32 pp.
- Smith, G.N., Smith, I.G.N., 1998. *Elements of Soil Mechanics*. Blackwell Science, Oxford. 494 pp.
- Van Asch, Th.W.J., Malet, J.-P., Remaître, A., Maquaire, O., 2004. Numerical modelling of the run-out of a muddy debris-flow. The effect of rheology on velocity and deposit thickness along the run-out track. Proceedings of the 9th International Symposium on landslides, Rio de Janeiro, Balkema, pp. 1433–1439.
- Wang, W.F., Sassa, K., 2003. Pore pressure generation and movement of rainfall induced landslides: effect of grain size and fine particle content. *Engineering Geology* 69, 109–125.
- Yoshimimi, Y., Tanaka, K., Tokimatsu, K., 1989. Liquefaction resistance of partially saturated sand. *Journal of Soil and Foundation Engineering* 29 (3), 157–162.